

Stars were born in significantly denser regions in the early Universe

M. Shirazi, J. Brinchmann and A. Rahmati

Leiden Observatory, Leiden University, P.O. Box 9513, 2300 RA Leiden, The Netherlands

shirazi@strw.leidenuniv.nl

ABSTRACT

The density of the warm ionized gas in high-redshift galaxies is known to be higher than what is typical in local galaxies on similar scales. At the same time, the mean global properties of the high- and low-redshift galaxies are quite different. Here, we present a detailed differential analysis of the ionization parameters of 14 star forming galaxies at redshift 2.6–3.4, compiled from the literature. For each of those high-redshift galaxies, we construct a comparison sample of low-redshift galaxies closely matched in specific star formation rate and stellar mass, thus ensuring that their global physical conditions are similar to the high-redshift galaxy. We find that the median $\log[\text{O II}] 3727/[\text{O III}] 5007$ line ratio of the high-redshift galaxies is 0.5 dex higher than their local counterparts. We construct a new calibration between the $[\text{O II}] 3727/[\text{O III}] 5007$ emission line ratio and ionization parameter to estimate the difference between the ionization parameters in the high and low-redshift samples. Using this, we show that the typical density of the warm ionized gas in star-forming regions decreases by a median factor of 8 from $z \sim 3.3$ to $z \sim 0$ at fixed mass and specific star formation rate. We show that metallicity differences can not explain the observed density differences. Because the high- and low-redshift samples are comparable in size, we infer that the relationship between star formation rate density and gas density must have been significantly less efficient at $z \sim 2 - 3$ than what is observed in nearby galaxies with similar levels of star formation activity.

Subject headings: galaxies: evolution — galaxies: high-redshift — galaxies: ISM — galaxies: star formation

1. Introduction

The cosmic star-formation rate, averaged over all observed galaxies in the Universe, has dropped by a factor of > 10 during the last ~ 10 Gyr (e.g., Hopkins & Beacom 2006). In addition to the increasing fraction of actively star-forming galaxies with increasing look-back time, the star-formation rates of typical galaxies increases rapidly towards the earlier stages of galaxy formation (Noeske et al. 2007; Daddi et al. 2007; Elbaz et al. 2007; Elbaz et al. 2011). Several studies also

provide hints that star formation conditions in distant galaxies (i.e., $z \sim 2 - 3$) are significantly different from the nearby Universe: emission lines from ionized gas in and around star-forming regions show different characteristics in distant and nearby galaxies (Brinchmann et al. 2008b; Liu et al. 2008; Newman et al. 2013), actively star-forming galaxies show higher gas fractions at higher redshifts (Tacconi et al. 2010; Genzel et al. 2010) and clumpy star-forming disks become increasingly more prevalent at higher redshifts (Cowie et al. 1995; Elmegreen & Elmegreen 2006; Genzel et al. 2011). The average density of the warm ionized gas in typical high-redshift (high- z) galaxies is also known to be significantly higher than in typical low-redshift (low- z) galaxies on similar scales (Elmegreen et al. 2009; Lehnert et al. 2009; Le Tiran et al. 2011; Newman et al. 2012; Tacconi et al. 2013; Lehnert et al. 2013).

These studies have revealed that distant star-forming galaxies form a population of objects that are distinct from their nearby analogs. However, it is unclear whether the main difference between low- z and high- z star-forming galaxies is related to their strongly evolving global properties, such as stellar mass (e.g., Ilbert et al. 2013; Muzzin et al. 2013), star formation rate (e.g., Noeske et al. 2007; Daddi et al. 2007; Elbaz et al. 2007; Elbaz et al. 2011) or metallicity (e.g., Mannucci et al. 2010; Lara-López et al. 2010), or that the interstellar medium (ISM) conditions were significantly different in similar galaxies at high- z . Comparing representative samples of high- z and low- z star-forming galaxies (e.g. Rigby et al. 2011) cannot disentangle the evolution in global characteristics from the possibly evolving star-formation conditions. We address this issue by selecting a comparison ensemble of low- z galaxies for each high- z star-forming galaxy in our sample, ensuring that the stellar mass and star-formation activities are similar in our high- z galaxies and their low- z comparison samples. This allows us to evaluate the differences in star-formation conditions between the high- z star-forming galaxies and their local analogs.

Although observations of some lensed galaxies at high- z reach spatial resolutions of ~ 100 pc (e.g., Swinbank et al. 2009; Jones et al. 2010), even this spatial resolution is insufficient to directly compare the small-scale properties of the ISM in high- z and low- z star-forming galaxies. However, these properties can be constrained through their impact on the emission line spectra of galaxies (e.g., Yeh & Matzner 2012). Here we use emission line ratios to derive the average ionization parameter of star-forming regions. Since the ionization parameter is a measure of ionizing radiation intensity per unit density, we can use it to constrain the density of star-forming regions in distant galaxies and compare it with that of their nearby counterparts.

The structure of the paper is as follows. In Section 2 we introduce our high- z sample and explain how we select their low- z counterparts. In Section 3 we introduce our new calibration for calculating the ionization parameter using the emission line ratios. We present our main results in Section 4 and compare the density of ionized gas in high- z and nearby galaxies. In Section 5 we investigate the impact of metallicity variations between the high- z and local galaxy samples on our results. We discuss the implications of our finding in Section 6 and end the paper with concluding remarks in Section 7.

2. Data

We have assembled a sample of 14 high- z star-forming galaxies from the literature for which published $[\text{O II}] \lambda 3727$, $[\text{O III}] \lambda 5007$ and $\text{H}\beta$ emission line fluxes are available (they have $[\text{O III}] \lambda 5007/\text{H}\beta > 0$). This sample consists of 2 galaxies (RXJ1053, Cl0949) from Richard et al. (2011, R11); 7 galaxies from the AMAZE sample (Maiolino et al. 2008, M08); 4 galaxies from the LSD sample (Mannucci et al. 2009, M09), and the 8 o’clock arc (Dessauges-Zavadsky et al. 2011; Shirazi et al. 2013, *arc*). These galaxies span redshifts between $z = 2.39$ and $z = 3.69$ with a median redshift of $z = 3.39$. All these galaxies also have gas metallicity, stellar mass and star-formation rate estimates. To test our results further, we also use a sample of 3 galaxies in the SINS survey (Förster Schreiber et al. 2009, 2011) that have directly measured electron densities using $[\text{S II}]$ doublet (Lehnert et al. 2009). The physical properties of our high- z sample are summarized in Table 1.

We compare these galaxies to matched samples of low- z galaxies from the Sloan Digital Sky Survey (SDSS) (York et al. 2000). We used the MPA-JHU¹ value added catalogues (Brinchmann et al. 2004; Tremonti et al. 2004) for SDSS DR7 (Abazajian et al. 2009) as our parent sample and selected star-forming galaxies following Brinchmann et al. (2004), with the adjustments of the line flux uncertainties given in Brinchmann et al. (2013). Furthermore, we used SDSS DR8 (Aihara et al. 2011) photometry to estimate stellar masses. The median and 1- σ scatter of the physical properties of the low- z sample of each high- z galaxy are summarized in Table 2.

As argued above, it is essential to take out correlations with global properties of galaxies when comparing their ISM conditions. To achieve this we select, for each high- z galaxy, all star-forming galaxies in the SDSS DR7 that have $\log M_*$ and $\log \text{SFR}/M_*$ within 0.3 dex of that of the high- z galaxy. We require that the SDSS galaxies to have $z > 0.02$ so that $[\text{O II}] \lambda 3727$, 29 are measured, they also have $[\text{O III}] \lambda 5007/\text{H}\beta > 0$. We note that for two galaxies in our high- z sample that have very high sSFR ($\sim 0.3 \text{ Gyr}^{-1}$), we had to include low- z galaxies whose $\log \text{SFR}/M_*$ differ by up to 1 dex to find a local analog sample. By default, we do not explicitly constrain the low- z samples to match the metallicity and/or size of their high- z counterparts as this would reduce the size of our sample and in the case of metallicity is subject to systematic uncertainties (e.g. Kewley & Ellison 2008). However, as we show below, matching metallicities and/or sizes does not affect our results significantly.

Any significant contribution of ionizing radiation from an Active Galactic Nucleus (AGN) could bias our estimates of the ionization parameter. For the low- z sample we can exclude strong AGN using the BPT diagram (Baldwin, Phillips & Terlevich 1981). At high- z , the galaxies from M08 and R11 do not show any evidence indicating the presence of AGNs in their rest frame UV spectra (i.e., $[\text{N V}]$, $[\text{C IV}]$, He II or broad $\text{Ly}\alpha$), X-ray and 24 μm Spitzer-MIPS observations (Maiolino et al. 2008; Richard et al. 2011; Shirazi et al. 2013). The LSD galaxies also show no evidence of AGN activity

¹<http://www.mpa-garching.mpg.de/SDSS/DR7>

in X-ray observations (Mannucci et al. 2009). While the aforementioned arguments do not rule out the presence of some AGN activity that is optically thick for X-rays, this is unlikely to significantly influence the optical emission lines which originate in only moderately obscured regions. One galaxy from the SINS sample (Q2343-BX610) that we use in this study has an indication of possible AGN from mid-IR observations (Förster Schreiber et al. 2011; Hainline et al. 2012) and from an analysis of resolved spectroscopy presented by Newman et al. (2013). However, we note that we do not use our calibration to infer ionization parameter for the SINS galaxies. Thus, we conclude that AGN activity is unlikely to bias our results at high- z .

3. Methodology

The high- z galaxies all have measured $[\text{O III}] \lambda 5007$ and $[\text{O II}] \lambda 3727$ line fluxes. This allows us to use the strong sensitivity of the $[\text{O III}] \lambda 5007 / [\text{O II}] \lambda 3727$ (hereafter O32) ratio to the ionization parameter (Penston et al. 1990) to estimate this. Kewley & Dopita (2002) derived an estimator for the ionization parameter using the dereddened O32 ratio. Since this can not easily be applied to our high- z sample in the absence of reliable reddening estimates, we here calibrate a new relation between the ionization parameter and the observed O32 ratio using the Charlot & Longhetti (2001, hereafter CL01) models that account for variations in dust properties and metallicities (see Table 4 in Shirazi & Brinchmann (2012) for the CL01 model grid used in our study). The effective ionization parameter in these models is taken to be the volume average over the Strömgren sphere (see equation 9 and 10 in CL01).

We wish to construct a calibration between the ionization parameter and O32 ratio that treats the metallicity as a free parameter. Based on this approach, as long as our high- z and low- z samples do not differ greatly in metallicity we do not need to know this exactly. We discuss this assumption further below, but given that we still have several possible ways to construct the calibration from the CL01 models:

a- Leaving all parameters in the CL01 models as free parameters in the fitting procedure (including all dust attenuation parameters, $0.01 < \tau_V < 4$). This is likely to give a large amount of scatter in the relationship.

b- Using only models with $\tau_V \sim 0.2$ and leaving all other model parameters free. This fit is appropriate if line ratios are corrected for dust attenuation but there is no constrain on the dust-to-metal ratio (ξ).

c- Using only models with $\tau_V \sim 0.2$ and $\xi \sim 0.3$ (i.e., the Galactic dust-to-metal ratio) and leaving all other model parameters free. Since ξ is expected to evolve weakly with time (Calura et al. 2008), it is reasonable to fix its value.

d- Using $\xi \sim 0.3$ and leaving all other model parameters free. Since ξ is likely not to differ strongly from this value, this is the best choice for a calibration when the amount of dust attenuation

is unknown.

These fits are plotted in Figure 1 from the top-left to the bottom-right, respectively. The best fits for the relation between ionization parameter and $\text{Log } [\text{O III}] \lambda 5007 / [\text{O II}] \lambda 3727$ (Log O32) are summarised as equation 1 to 4, respectively. We use option *d*, Equation 4, as our reference in this study because in general we do not have enough information to accurately constrain the dust attenuation for the high-*z* galaxy sample. To derive our reference relation we fix $\xi = 0.3$, which is the Galactic value (see Brinchmann et al. 2013, for a discussion), and allow all other parameters to vary. We use the same fit for estimating the ionization parameter for low-*z* counterparts of high-*z* galaxies.

$$\text{Log } U = -3.300 \pm 0.017 + (0.481 \pm 0.019) \text{Log O32} \quad (1)$$

$$\text{Log } U = -3.109 \pm 0.039 + (0.586 \pm 0.039) \text{Log O32} \quad (2)$$

$$\text{Log } U = -3.119 \pm 0.027 + (0.804 \pm 0.035) \text{Log O32} \quad (3)$$

$$\text{Log } U = -3.363 \pm 0.011 + (0.593 \pm 0.012) \text{Log O32} \quad (4)$$

We are primarily focused on relative statements in this work so the most important aspect of these calibrations is how they convert relative statements in O32 to relative statements about $\log U$. Since the slope in equation 1, 2 & 4 is similar they will result in similar relative statements about $\log U$, while that in equation 3 is even steeper and would lead to an even stronger result than that outlined below.

4. Results

The left and middle panels of Figure 2 compare the $[\text{O III}] \lambda 5007 / [\text{O II}] \lambda 3727$ ratios and corresponding ionization parameters (from Equation 4) for our high-*z* sample (colored symbols), and the median values of their low-*z* analogs (black circles). Error bars shown on the black circles indicate 1- σ scatter in the low-*z* sample of each high-*z* galaxy. It is evident that the high-*z* star-forming galaxies show significantly higher $[\text{O III}] \lambda 5007 / [\text{O II}] \lambda 3727$ ratios (up to ≈ 0.8 dex higher) compared to their low-*z* analogs. This translates into significantly higher ionization parameters (up to ~ 0.5 dex) in the high-*z* galaxies relative to low-*z* even though their star formation rates and masses are constrained to be the same.

For a given production rate of hydrogen ionizing photons, Q , and after assuming that most of ionizing photons are absorbed locally, the ionization parameter in a typical ionized region can be related to the hydrogen number density, n_{H} :

$$U^3 \propto Q(t) n_{\text{H}} \epsilon^2, \quad (5)$$

where ϵ is the volume filling factor of the ionized gas, which is defined as the ratio between the volume-weighted and mass-weighted average hydrogen densities (Charlot & Longhetti 2001). This

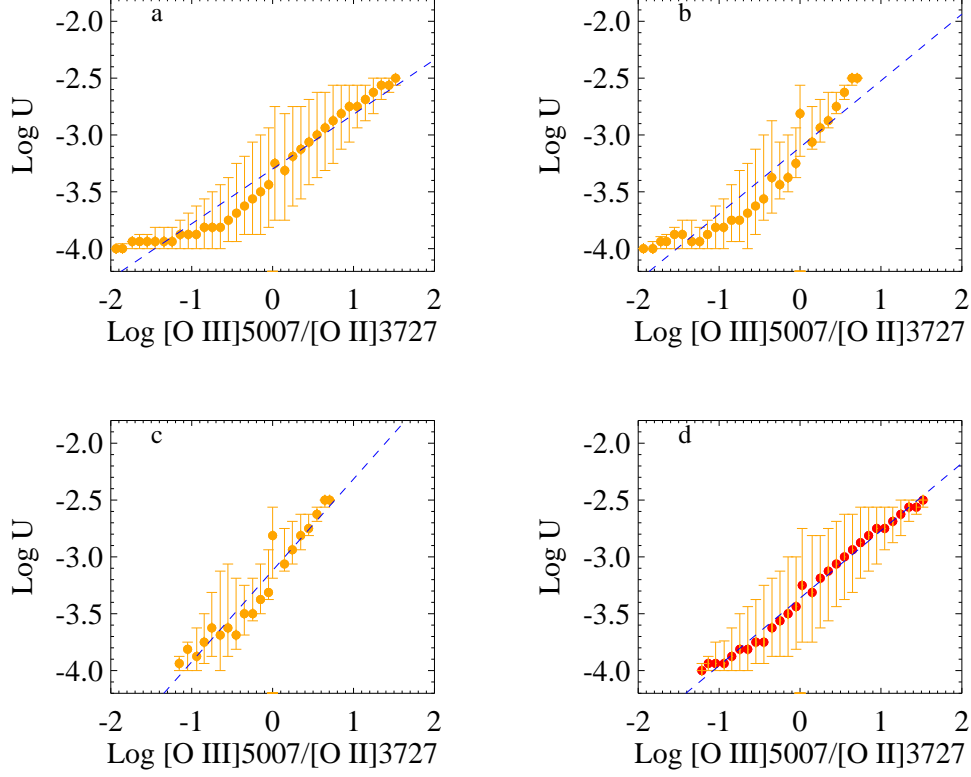


Fig. 1.— Best-fit relations between ionization parameters and the $[\text{O III}] \lambda 5007/[\text{O II}] \lambda 3727$ (O32) ratios are shown by blue dashed lines. The top-left panel shows the best-fit using all CL01 models ($0.01 < \tau_V < 4$), on the top-right we show the best-fit using only models with $\tau_V \sim 0.2$, the bottom-left panel shows the best-fit using only models with $\tau_V \sim 0.2$ and $\xi \sim 0.3$ (i.e., Galactic dust-to-metal ratio), and in the bottom-right panel we show the best-fit to all models with $\xi \sim 0.3$. The results in the paper are presented for the fit shown in the lower-right panel.

allows us to constrain the densities of star-forming regions, by measuring their ionization parameters.

Assuming that the production rate of hydrogen ionizing photons and volume filling factors of the ionized gas are similar in typical star-forming regions in high- z galaxies and their low- z analogs, one can translate the ratio between the ionization parameters of the high- z galaxies and their low- z counterparts into the ratio of their ionized gas densities. The difference between the density of the ionized gas in star-forming regions in our high- z galaxies and their low- z analogs is shown in the right panel of Figure 2. This shows up to ≈ 25 times higher densities in high- z star-forming galaxies.

To derive physical densities for our high- z galaxies from the relative density differences shown in Figure 2, we exploit the fact that for the nearby galaxies we can estimate the electron density from the [S II] $\lambda 6716, 6731$ ratio and thus get an estimate of the electron density in the high- z galaxies. The resulting absolute densities for the ionized gas in our high- z star-forming galaxies are shown in Figure 3. The median values of the electron densities of the low- z samples, inferred from the [S II] $\lambda 6716, 6731$ doublet, are shown by the black filled circles in the figure where error bars show $1\text{-}\sigma$ scatter. The median values of the redshifts of the low- z samples and the number of low- z analogs in each sample are indicated with n in the figure. Colored symbols show our high- z sample with their redshifts indicated. The high- z values are inferred from the low- z values multiplied by $n_e(z)/n_e(z=0)$ ratios shown in Figure 2, and their error bars show propagation of uncertainties based on Equation 4. The grey small dashed and long dashed lines show the median values for the electron density at low- z and high- z , respectively.

Besides the sensitivity of the ionization parameter to the density of the emitting gas, it also depends on the production rate of ionizing photons and the volume filling factor of the ionized gas (Charlot & Longhetti 2001). Therefore, our density estimates might also be sensitive to the possible differences in the ionizing photons production rate and the volume filling factor of the ionized gas between high- z and nearby galaxies. To address this concern, in Figure 3 we show electron densities for a sample of five high- z star-forming galaxies in the SINS survey (Förster Schreiber et al. 2009; Lehnert et al. 2009) as purple diamonds. The electron density for these galaxies has been measured directly using the [S II] $\lambda 6716, 6731$ doublet and is in a good agreement with our inferred evolution in density estimated from the ionization parameter. For three of these five objects that have available stellar masses and specific star formation rates (Förster Schreiber et al. 2011), we constructed low- z analog samples. The comparison between the electron density of these three objects and their low- z analogs also shows good agreement (evolution in density with a median factor of 8.4) with the density ratios we obtained for our high- z star-forming galaxies using their ionization parameters (an evolution in density with a median factor of 7.9). This further strengthens our argument that an elevated density of star-forming regions in high- z galaxies is the main reason for their higher ionization parameter.

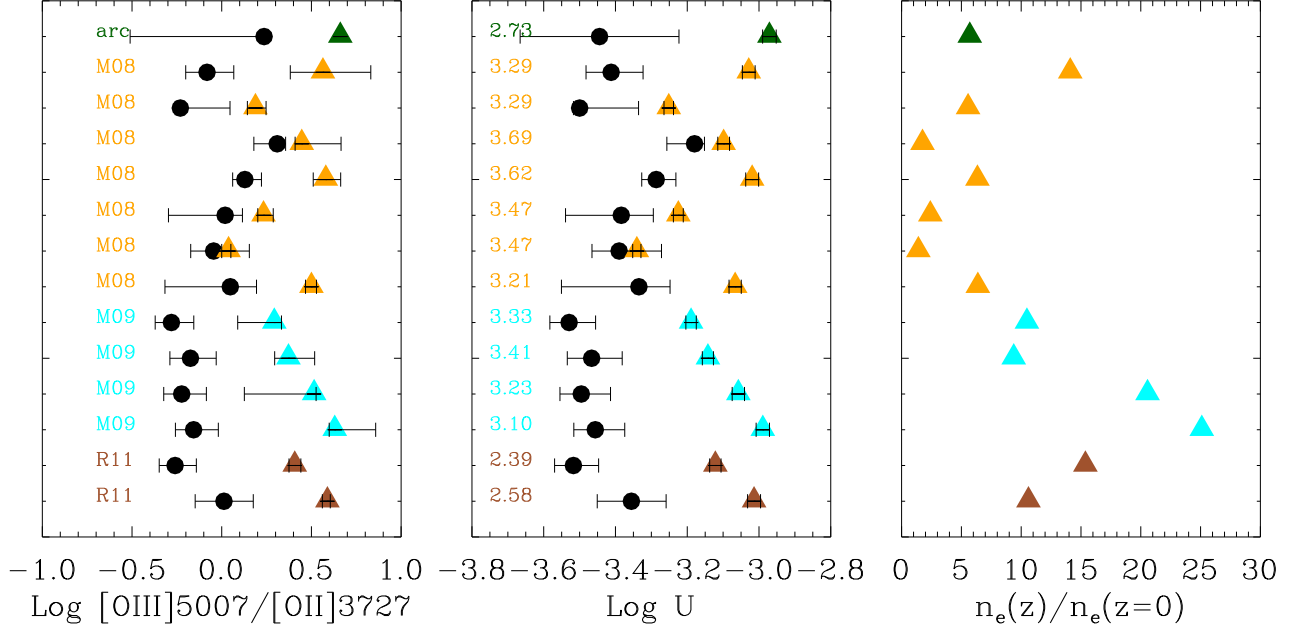


Fig. 2.— A comparison between [O III] $\lambda 5007$ /[O II] $\lambda 3727$ ratio, ionization parameter and electron density at low-z and high-z. The x-axis on the left panel shows the [O III] $\lambda 5007$ /[O II] $\lambda 3727$ ratio, the middle panel shows the ionization parameter and the right panel shows the electron density at high-z relative to that of low-z. Colored symbols show high-z galaxies with their redshift indicated and black circles show the median values for the low-z sample of each high-z galaxy. Error bars span from the 16% to the 84% confidence level. We see that high-z galaxies show higher [O III] $\lambda 5007$ /[O II] $\lambda 3727$ ratios than their low-z analogs (up to ≈ 0.8 dex higher), even though their masses and sSFR are the same. The middle panel shows the ionization parameters derived using our new calibration between the [O III] $\lambda 5007$ /[O II] $\lambda 3727$ ratio and the ionization parameter. We see that high-z galaxies show up to ~ 0.5 dex higher (median ~ 0.3 dex) ionization parameters than their low-z analogs. This translates to up to 25 times higher electron density for high-z galaxies relative to their low-z analogs.

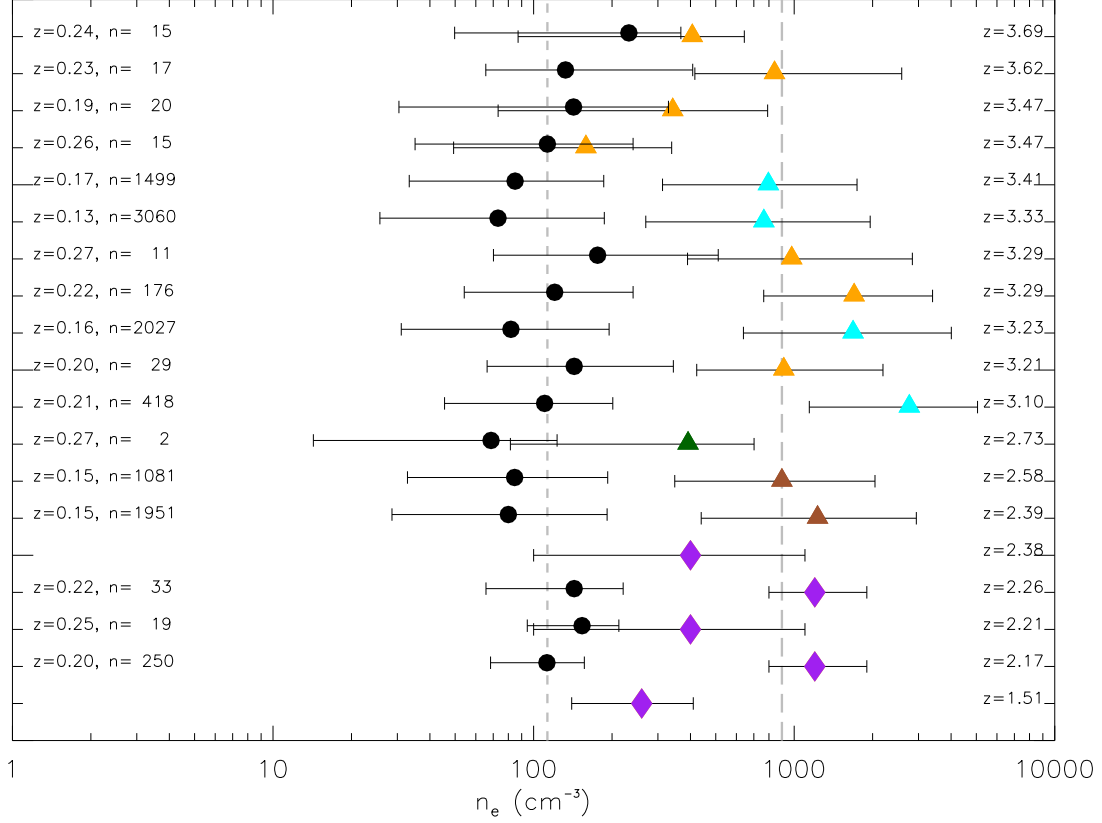


Fig. 3.— The median value of the electron density for the low- z samples inferred from the [S II] 6716, 6731 doublet is shown by the black filled circles. The high- z values are inferred from the low- z values multiplying by $n_e(z)/n_e(z=0)$ ratios shown in Figure 2. Colored symbols show our high- z sample sorted based on their redshifts from down to top as indicated on the figure. Five galaxies from the SINS survey that have directly measured electron densities are shown by purple diamonds. The median values of the redshifts of low- z samples are shown in black and the number of low- z analogs in each sample are indicated with n . Error bars span from the 16% to the 84% confidence level (low- z data: they show scatter in the sample, high- z data: they show propagation of uncertainties through Equation 4). The grey small dashed and long dashed lines show the median value for the electron density at low- z and high- z , respectively.

5. Metallicity dependence

A key result in this work is that high- z galaxies have a typically 0.5 dex higher Log O32 than low- z galaxies with the same mass and sSFR. We interpret this as primarily being due to a difference in ionization parameter but O32 is also sensitive to metallicity. Ideally we would select our high- z and low- z samples to have the same metallicity but to do this we require a metallicity estimator that can be applied equally at low- z and high- z allowing for a variation in ionization parameter. With the current data available for high- z galaxies this is not possible, thus we need to assess whether metallicity differences between the samples could be the reason for the observed offset.

Mannucci et al. (2010) and Lara-López et al. (2010) showed that there is a relationship between stellar mass, metallicity and star formation rate (SFR) that appear to hold to high- z ($z < 2.5$ for Mannucci et al. and $z < 3.5$ for Lara-Lopez et al.). Therefore, if this holds for our galaxies, a selection on stellar mass and SFR should ensure that the metallicity difference between the high- and low- z sample is small. Given our small sample and considering that Mannucci et al. (2010) argued that the multi-parameter relationship was not well established at $z > 2.5$, where most of our high- z galaxies lie, it is necessary to examine this assumption more carefully. It is useful to start this by asking what metallicity difference would give a O32 difference similar to what is observed. From Brinchmann et al. (2008b, their Figure 8), or directly using the CL01 models, we find that a change in metallicity from $1 Z_{\odot}$ to $0.1 Z_{\odot}$ leads to a change in Log O32 of 0.40 ± 0.07 dex. Thus we need a major difference in metallicity to explain the results.

We can test for a large offset in metal content by calculating the metallicities of the high- and low- z samples in a consistent way. To do this we adopt the methodology used for AMAZE and LSD described in (Maiolino et al. 2008) for both high- and low- z galaxies. Note that, by construction, this method assumes that all variation in O32 is due to metallicity. Therefore, by using it, we will maximize the contribution of metallicity to the change in O32 and hence derive a minimum difference in ionization parameter between the low- and high- z objects. Based on the derived metallicities, we can calculate the maximum difference in O32 between high- and low- z galaxies due to metallicity differences, using the CL01 models and by averaging over U . This gives us the expected change in O32 due to metallicity only, and we subtract this off the actually observed difference for each galaxy.

The resulting difference can be seen in the top panel of Figure 4. We emphasize that since we have used an abundance calibration that assumes that changes in O32 are due to metallicity, this correction should be the maximum possible correction. This gives a lower limit to the difference in O32 between high- and low- z galaxies and it is still quite sizeable. Converting this to a density difference as done in the main text we get the lower panel in that figure. This shows that the mean (median) electron density of the high- z galaxies is 5.5 (3.5) times higher than the low- z galaxies with the same sSFR and mass.

To test further the sensitivity of our results to metallicity differences between our high- z galax-

ies and their low- z analogs, we made a low- z comparison sample for all high- z galaxies ensuring that their metallicities were equal to within 0.3 dex, in addition to matching their stellar masses and sSFRs². In this case we found that high- z galaxies show a median of ≈ 6.1 higher density compared to their low- z analogs with similar sSFRs, masses and metallicities; a result which is not significantly different from what we found without matching metallicities.

We also note that the densities that are measured directly from the [S II] doublet for the 5 high- z galaxies we selected from the SINS, are not derived using our calibration and hence are insensitive to variations in metallicity. Yet they have densities which are on average 8.4 times higher than their local analogs. It also worth noting that not all SINS galaxies have detected [S II] which is consistent with these conclusions because [S II]/H α decreases with increasing U at fixed metallicity (e.g., Brinchmann et al. 2008a, their Figure 11).

In conclusion, regardless of how we correct for possible differences in metallicity between the high- and low- z samples, the effect is minor and the main result of the paper is robust to these corrections. Thus we conclude that differences in metallicity can not explain the observed major offset in O32 and that systematic differences in the ionization parameter is the main cause.

6. Discussion

The observed strong evolution in the global properties such as star formation intensity, stellar mass and size indicates that mean star formation conditions are different in distant galaxies compared to typical galaxies today (Cowie et al. 1995; Elmegreen & Elmegreen 2006; Noeske et al. 2007; Daddi et al. 2007; Elbaz et al. 2007; Elbaz et al. 2011; Tacconi et al. 2010; Genzel et al. 2010, 2011). In this work we have however shown that even when the star formation intensity and mass are the *same*, the density in the ionized gas in high- and low- z galaxies differ dramatically. This difference would naturally imply a higher pressure in the colder ISM surrounding the ionized gas (Dopita et al. 2006), and thence its higher density.

This could naturally occur if star formation at high- z was more concentrated to the central regions, so to check this we compared the u-band half-light radius for the SDSS galaxies with the half-light radius of the high- z galaxies when they are available (for 7 galaxies). Among the high- z galaxies, only one has a smaller size than the median size of its low- z counterparts. This is in agreement with the findings of Lehnert et al. (2009) and can not explain the density differences seen for any reasonable mass profile in the galaxies. We double-checked this by constructing a matched low- z sample that have $\log \text{SFR}/\pi r_{1/2}^2$ within 0.3 dex of their high- z counterparts where $r_{1/2}$ is the half-light radius. This results in a median density difference greater than 19 between low- z and high- z galaxies compared to a median difference of ~ 8 before matching SFR densities. This shows that size differences are unlikely to be the explanation of the systematic differences.

²Note that this additional metallicity constraint decreases the low- z sample sizes.

We have not required a match in SFR density in the bulk of the paper. However, because the size definitions are somewhat arbitrary and we do not have sizes for all galaxies at high- z .

Assuming now that the distribution of star formation is comparable at low- and high- z , we next assume that the H II regions are in pressure equilibrium with their surrounding ISM (Oey & Clarke 1997; Dopita et al. 2006). Under this assumption the increased pressure in the ionized regions implies a higher pressure in the cold ISM. There are considerable uncertainties in how ionized regions expand in detail. However, in our case it is not unreasonable to assume that those complexities should be similar at high and low redshift. This is because the evolution of the H II regions is driven by the energy injection from massive stars which should be similar at high- z and low- z , given how we selected our samples. The same applies to cosmic ray production rates which contribute to the heating (and the pressure support) of the ambient ISM. Note that this also means that the contribution of radiation pressure to the equilibrium for the H II regions (Yeh & Matzner 2012, e.g.) should be similar at low and high redshift.

It is hard to test whether the H II regions in the high- z galaxies have reached pressure equilibrium with their surrounding ISM. However, since the mechanical input energy is the same at high and low redshift, and the life-times of the relevant stellar population is also the same, it seems unlikely that the evolutionary age of the H II regions differs significantly between the high- z and low- z samples. This is also supported by Verdolini et al. (2013) who used a population study to show that the line emission of a galaxy will typically be dominated by the youngest H II regions. Verdolini et al. (2013) also show explicitly the effect of an elevated ambient pressure on emission line ratios (their Figure 8), which is a qualitatively similar trend to what we infer here.

Thus, the simplest explanation for the elevated density in the high- z H II regions is an elevated pressure in the cold ISM relative to similar galaxies nearby. This increased pressure could arise from various sources, but in general, one would expect a pressure-density relation, $P \propto \rho^\gamma$ with $\gamma > 1$. Thus, the increased pressure would correspond to an increased ISM density by an amount that depends on the model adopted for the ISM and we do not attempt to discuss this in detail here. The simplest model, where the ISM temperature is the same at high and low redshift, would predict that the density difference between the ISM at high- and low- z would be the same as that of the ionized regions, i.e., $\rho_{\text{high-}z} \sim 8 \rho_{\text{low-}z}$.

This conclusion has important implications for empirical star-formation law as well. The most popular scaling relation observed between star formation activity and gas surface density in the local Universe is the Kennicutt-Schmidt relation (Kennicutt 1998),

$$\Sigma_{\text{SFR}} \propto \Sigma_{\text{gas}}^{1.4}, \quad (6)$$

where Σ denote surface densities. In our case Σ_{SFR} is approximately the same in the high- and low- z galaxies (see above), but the gas density is much higher. If the scale-height of the gas is not significantly smaller in high- z galaxies, one can conclude that the scaling relation in the high- z galaxies is significantly different from what is observed in their low- z counterparts, being a factor ~ 5 – 8 less efficient.

We note however that we can not distinguish between molecular and atomic gas. Our results therefore are for the total gas and we cannot directly compare them to molecular studies (e.g., Daddi et al. 2010; Tacconi et al. 2013) at high- z and leave a discussion of this for future work.

7. Conclusion

In this work we compare the physical conditions of the ISM in high- z galaxies and their low- z counterparts which are selected to have similar global properties as that of high- z galaxies. This selection criteria minimize the differences between distant and nearby galaxies due to the evolution of the global properties such as mass and sSFR from high- z to low- z and can therefore be used to study the evolution of intrinsic properties of the ISM.

Previous studies have already pointed out that the physical densities/properties of the star-forming regions at high- z are very different from those in the local Universe and we confirm this here. Using a novel approach, we have been able to go one step further, and show that this difference can not fully be explained by an increased star formation activity in the high redshift galaxies. Since we compare high and low- z galaxies that are matched in sSFR, their different densities must reflect an intrinsic difference in ISM conditions between high and low- z . We argue that this difference is primarily due to a difference in the density of the warm ionized gas. We have also shown that the differences between the high- and low- z galaxies can not be explained by differences in metallicity. By showing that the high- z and low- z samples are also comparable in size, we conclude that the relationship between star formation rate density and gas density must have been significantly less efficient at $z \sim 2 - 3$ than what is observed locally. This, in turn, implies that most of the stars in the local Universe were formed following a different star formation scaling relation than what is observed in normal galaxies today.

Acknowledgments

We thank Marijn Franx for helpful discussion. We also thank Leslie Sage and the two anonymous referees for very useful comments which improved this paper.

REFERENCES

- Abazajian, K. N., Adelman-McCarthy, J. K., Agüeros, M. A., et al. 2009, *ApJS*, 182, 543
- Aihara, H., Allende Prieto, C., An, D., et al. 2011, *ApJS*, 193, 29
- Baldwin, J. A., Phillips, M. M., & Terlevich, R. 1981, *PASP*, 93, 5
- Brinchmann, J., Charlot, S., Kauffmann, G., et al. 2013, *MNRAS*, doi:10.1093/mnras/stt551

Table 1. High-z sample.

ID	Name	z	Log Mass M_{\odot}	Log sSFR yr^{-1}	SFR $M_{\odot} yr^{-1}$	Σ_{SFR} $M_{\odot} yr^{-1} kpc^{-2}$	$r_{1/2}$ kpc	Log O32	12 + LogO/H	Log U	n_e cm^{-3}
R11	RXJ1053	2.576	$9.62^{0.75}_{-0.72}$	-8.66	$9.1^{2.3}_{-2.3}$	0.22	3.62 ± 0.45	$0.589^{0.0}_{-0.0}$	$8.68^{0.11}_{-0.12}$	$-3.01^{0.02}_{-0.02}$	$897.3^{1145.2}_{-549.2}$
R11	Cl0949	2.394	$10.19^{0.22}_{-0.18}$	-9.31	$7.5^{1.5}_{-1.5}$	0.19	3.50 ± 0.88	$0.407^{0.0}_{-0.0}$	$8.10^{0.06}_{-0.05}$	$-3.12^{0.02}_{-0.02}$	$1229.4^{1713.1}_{-789.8}$
M09	SSA22a-C30	3.103	$10.33^{0.31}_{-0.38}$	-8.87	$29.0^{81.0}_{-21.0}$	4.21	1.48 ± 0.44	$0.630^{0.2}_{-0.0}$	$8.16^{0.20}_{-0.60}$	$-2.99^{0.02}_{-0.02}$	$2766.6^{2286.8}_{-1623.8}$
M09	Q0302-C131	3.235	$10.09^{0.10}_{-0.33}$	-9.09	$10.0^{6.0}_{-4.0}$	1.97	1.27 ± 0.37	$0.515^{0.0}_{-0.4}$	$8.00^{0.25}_{-0.40}$	$-3.06^{0.02}_{-0.02}$	$1682.9^{2325.3}_{-1044.2}$
M09	Q0302-M80	3.414	$10.07^{0.23}_{-0.19}$	-8.96	$13.0^{17.0}_{-8.0}$	7.36	0.75 ± 0.24	$0.372^{0.1}_{-0.1}$	$8.36^{0.15}_{-0.15}$	$-3.14^{0.02}_{-0.02}$	$796.2^{946.5}_{-483.8}$
M09	Q0302-C171	3.328	$10.06^{0.10}_{-0.28}$	-9.36	$5.0^{2.0}_{-2.0}$	1.02	1.25 ± 0.39	$0.293^{0.0}_{-0.2}$	$8.14^{0.25}_{-0.45}$	$-3.19^{0.01}_{-0.01}$	$765.1^{1192.4}_{-495.7}$
M08	CDFa-C9	3.212	$10.18^{0.40}_{-0.08}$	-7.76	$265.0^{0.0}_{-0.0}$	$0.500^{0.0}_{-0.0}$	$8.10^{0.18}_{-0.21}$	$-3.07^{0.02}_{-0.02}$	$912.6^{1278.7}_{-489.9}$
M08	CDFS-4414	3.471	$10.57^{0.19}_{-0.22}$	-8.52	$113.0^{0.0}_{-0.0}$	$0.038^{0.0}_{-0.0}$	$8.54^{0.15}_{-0.14}$	$-3.34^{0.01}_{-0.01}$	$158.8^{179.9}_{-109.5}$
M08	CDFS-4417	3.473	$10.29^{0.37}_{-0.11}$	-7.65	$438.0^{0.0}_{-0.0}$	$0.233^{0.0}_{-0.0}$	$8.55^{0.09}_{-0.10}$	$-3.22^{0.01}_{-0.01}$	$342.0^{448.9}_{-268.9}$
M08	CDFS-16767	3.624	$10.05^{0.10}_{-0.16}$	-8.13	$84.0^{0.0}_{-0.0}$	$0.580^{0.1}_{-0.1}$	$8.31^{0.11}_{-0.17}$	$-3.02^{0.02}_{-0.02}$	$840.7^{1746.3}_{-425.0}$
M08	CDFS-2528	3.688	$9.76^{0.09}_{-0.07}$	-7.76	$101.0^{0.0}_{-0.0}$	$0.446^{0.2}_{-0.0}$	$8.07^{0.39}_{-0.28}$	$-3.10^{0.02}_{-0.02}$	$406.5^{237.1}_{-319.3}$
M08	SSA22a-M38	3.294	$11.01^{0.18}_{-0.41}$	-8.95	$115.0^{0.0}_{-0.0}$	$0.188^{0.1}_{-0.0}$	$8.34^{0.15}_{-0.12}$	$-3.25^{0.01}_{-0.01}$	$978.5^{1862.6}_{-588.7}$
M08	SSA22a-aug16M16	3.292	$10.29^{0.20}_{-0.21}$	-8.67	$42.0^{0.0}_{-0.0}$	$0.564^{0.3}_{-0.2}$	$7.99^{0.26}_{-0.34}$	$-3.03^{0.02}_{-0.02}$	$1698.7^{1698.0}_{-934.8}$
arc	8oclock	2.735	$10.24^{1.80}_{-0.45}$	-7.88	$228.0^{10.0}_{-10.0}$	9.26	2.80 ± 0.20	0.661	$8.35^{0.19}_{-0.19}$	$-2.97^{0.02}_{-0.02}$	$391.5^{310.0}_{-310.0}$
SINS ^a	Q2343-BX389	2.172	$10.61^{0.77}_{-2.16}$	-9.22	1200.0^{700}_{-400}
SINS ^a	Q2343-BX610	2.210	$11.00^{2.70}_{-0.60}$	-9.22	400.0^{700}_{-300}
SINS ^a	Q2346-BX482	2.256	$10.26^{0.79}_{-0.46}$	-8.36	1200.0^{700}_{-400}

^aWe use the properties of the SINS galaxies that are given in Förster Schreiber et al. (2011) and Lehnert et al. (2009).

Table 2. Low-z sample.

High-z ID	$\langle z \rangle^a$	$\langle \text{Log Mass} \rangle$ M_\odot	$\langle \text{Log sSFR} \rangle$ yr^{-1}	$\langle \text{Log SFR} \rangle$ $M_\odot yr^{-1}$	$\langle \Sigma_{SFR} \rangle$ $M_\odot yr^{-1} kpc^{-2}$	$\langle r50_u \rangle$ kpc	$\langle \text{Log O32} \rangle$	$\langle 12 + \text{LogO/H} \rangle$ M08 calib ^b	$\langle \text{Log U} \rangle$	$\langle n_e \rangle$ cm^{-3}
RXJ1053	$0.15^{+0.07}_{-0.07}$	$9.59^{+0.20}_{-0.19}$	-8.81	$0.9^{+0.2}_{-0.3}$	1.91	$1.11^{+0.41}_{-0.24}$	$0.012^{+0.163}_{-0.161}$	$8.49^{+0.12}_{-0.05}$	$-3.36^{+0.10}_{-0.10}$	$84.6^{+107.9}_{-51.8}$
Cl0949	$0.15^{+0.07}_{-0.05}$	$10.04^{+0.19}_{-0.11}$	-9.32	$0.8^{+0.3}_{-0.3}$	0.93	$1.46^{+0.65}_{-0.42}$	$-0.260^{+0.118}_{-0.088}$	$8.70^{+0.05}_{-0.07}$	$-3.52^{+0.07}_{-0.05}$	$80.0^{+111.5}_{-51.4}$
SSA22a-C30	$0.21^{+0.05}_{-0.08}$	$10.18^{+0.19}_{-0.11}$	-9.03	$1.2^{+0.2}_{-0.2}$	3.70	$1.22^{+0.32}_{-0.27}$	$-0.157^{+0.138}_{-0.101}$	$8.65^{+0.07}_{-0.10}$	$-3.46^{+0.08}_{-0.06}$	$110.2^{+91.1}_{-64.7}$
Q0302-C131	$0.16^{+0.07}_{-0.05}$	$9.96^{+0.21}_{-0.12}$	-9.19	$0.8^{+0.2}_{-0.3}$	1.35	$1.32^{+0.54}_{-0.33}$	$-0.223^{+0.137}_{-0.100}$	$8.67^{+0.07}_{-0.09}$	$-3.50^{+0.08}_{-0.06}$	$81.8^{+113.1}_{-50.8}$
Q0302-M80	$0.17^{+0.06}_{-0.06}$	$9.94^{+0.21}_{-0.13}$	-9.08	$0.9^{+0.2}_{-0.2}$	1.86	$1.24^{+0.41}_{-0.29}$	$-0.174^{+0.143}_{-0.115}$	$8.64^{+0.08}_{-0.10}$	$-3.47^{+0.09}_{-0.07}$	$84.9^{+100.9}_{-51.6}$
Q0302-C171	$0.13^{+0.07}_{-0.05}$	$9.93^{+0.20}_{-0.12}$	-9.37	$0.6^{+0.3}_{-0.3}$	0.53	$1.53^{+0.84}_{-0.46}$	$-0.281^{+0.125}_{-0.090}$	$8.71^{+0.05}_{-0.08}$	$-3.53^{+0.07}_{-0.05}$	$73.0^{+113.8}_{-47.3}$
CDFa-C9	$0.20^{+0.07}_{-0.08}$	$10.05^{+0.15}_{-0.13}$	1.74	$-8.4^{+12.3}_{-9.9}$	17.63	$0.95^{+0.33}_{-0.95}$	$0.048^{+0.146}_{-0.364}$	$8.44^{+0.08}_{-8.44}$	$-3.33^{+0.09}_{-0.22}$	$143.1^{+200.6}_{-76.8}$
CDFS-4414	$0.26^{+0.03}_{-0.10}$	$10.42^{+0.21}_{-0.10}$	-8.70	$1.6^{+0.4}_{-0.2}$	12.18	$1.09^{+0.43}_{-0.17}$	$-0.045^{+0.199}_{-0.128}$	$8.57^{+0.13}_{-0.08}$	$-3.39^{+0.12}_{-0.08}$	$112.9^{+128.0}_{-77.9}$
CDFS-4417	$0.19^{+0.09}_{-0.10}$	$10.10^{+0.20}_{-0.08}$	1.90	$-8.0^{+11.9}_{-9.7}$	25.71	$0.91^{+0.39}_{-0.91}$	$0.019^{+0.096}_{-0.316}$	$8.44^{+0.13}_{-8.44}$	$-3.38^{+0.09}_{-0.16}$	$142.3^{+186.9}_{-111.9}$
CDFS-16767	$0.23^{+0.04}_{-0.05}$	$9.90^{+0.17}_{-0.11}$	-8.38	$1.6^{+0.2}_{-0.1}$	14.91	$1.06^{+0.21}_{-0.29}$	$0.129^{+0.092}_{-0.068}$	$8.45^{+0.10}_{-0.01}$	$-3.29^{+0.05}_{-0.04}$	$132.6^{+275.4}_{-67.0}$
CDFS-2528	$0.24^{+0.04}_{-0.09}$	$9.48^{+0.16}_{-0.02}$	-7.93	$1.7^{+0.1}_{-0.3}$	22.25	$0.83^{+0.34}_{-0.14}$	$0.309^{+0.047}_{-0.130}$	$8.41^{+0.05}_{-0.09}$	$-3.18^{+0.03}_{-0.08}$	$232.1^{+135.4}_{-182.3}$
SSA22a-M38	$0.27^{+0.02}_{-0.09}$	$10.86^{+0.23}_{-0.12}$	-9.02	$1.8^{+0.3}_{-0.3}$	3.72	$1.89^{+3.59}_{-0.72}$	$-0.231^{+0.277}_{-0.029}$	$8.71^{+0.04}_{-0.14}$	$-3.50^{+0.16}_{-0.02}$	$176.0^{+335.1}_{-105.9}$
SSA22a-aug16M16	$0.22^{+0.05}_{-0.09}$	$10.12^{+0.19}_{-0.10}$	-8.84	$1.4^{+0.2}_{-0.2}$	6.25	$1.17^{+0.28}_{-0.24}$	$-0.082^{+0.149}_{-0.119}$	$8.60^{+0.08}_{-0.12}$	$-3.41^{+0.09}_{-0.07}$	$120.5^{+120.4}_{-66.3}$
8oclock	$0.27^{+0.00}_{-0.22}$	$10.03^{+0.00}_{-0.07}$	-8.04	$1.8^{+0.0}_{-2.0}$	17.63	$3.01^{+0.00}_{-1.95}$	$0.236^{+0.000}_{-0.747}$	$8.78^{+0.00}_{-0.40}$	$-3.44^{+0.22}_{-0.22}$	$68.7^{+54.4}_{-54.4}$
Q2343-BX389	$0.20^{+0.05}_{-0.08}$	$10.44^{+0.17}_{-0.10}$	-9.27	$1.2^{+0.2}_{-0.2}$	2.49	$1.40^{+0.51}_{-0.36}$	$-0.205^{+0.113}_{-0.085}$	$8.70^{+0.04}_{-0.08}$	$-3.48^{+0.07}_{-0.05}$	112.5^{+127}_{-68}
Q2343-BX610	$0.25^{+0.02}_{-0.09}$	$10.84^{+0.27}_{-0.11}$	-9.27	$1.5^{+0.2}_{-0.1}$	5.23	$1.55^{+0.65}_{-0.52}$	$-0.197^{+0.140}_{-0.061}$	$8.71^{+0.04}_{-0.09}$	$-3.48^{+0.08}_{-0.04}$	153.5^{+228}_{-94}
Q2346-BX482	$0.22^{+0.06}_{-0.10}$	$10.07^{+0.13}_{-0.06}$	-8.55	$1.6^{+0.1}_{-0.1}$	12.15	$1.08^{+0.27}_{-0.20}$	$0.084^{+0.110}_{-0.087}$	$8.47^{+0.09}_{-0.03}$	$-3.31^{+0.07}_{-0.05}$	143.1^{+100}_{-65}

^a $\langle \rangle$ shows the median value where lower and upper values show $1 - \sigma$ scatter in the sample.

^bMetallicities are measured using Maiolino et al. (2008) calibration.

- Brinchmann, J., Charlot, S., White, S. D. M., et al. 2004, MNRAS, 351, 1151
- Brinchmann, J., Kunth, D., & Durret, F. 2008a, A&A, 485, 657
- Brinchmann, J., Pettini, M., & Charlot, S. 2008b, MNRAS, 385, 769
- Calura, F. and Pipino, A. and Matteucci, F., 2008, A&A, 479, 669
- Charlot, S., & Longhetti, M. 2001, MNRAS, 323, 887
- Cowie, L. L., Hu, E. M., & Songaila, A. 1995, AJ, 110, 1576
- Daddi, E., Dickinson, M., Morrison, G., et al. 2007, ApJ, 670, 156
- Daddi, E., Elbaz, D., Walter, F., et al. 2010, ApJ, 714, L118
- Dessauges-Zavadsky, M., Christensen, L., D’Odorico, S., Schaerer, D., & Richard, J. 2011, A&A, 533, A15
- Dopita, M. A., Fischera, J., Sutherland, R. S., et al. 2006, ApJ, 647, 244
- Elbaz, D., Daddi, E., Le Borgne, D., et al. 2007, A&A, 468, 33
- Elbaz, D., Dickinson, M., Hwang, H. S., et al. 2011, A&A, 533, A119
- Elmegreen, B. G., & Elmegreen, D. M. 2006, ApJ, 650, 644
- Elmegreen, D. M., Elmegreen, B. G., Marcus, M. T., et al. 2009, ApJ, 701, 306
- Förster Schreiber, N. M., Genzel, R., Bouché, N., et al. 2009, ApJ, 706, 1364
- Förster Schreiber, N. M., Shapley, A. E., Genzel, R., et al. 2011, ApJ, 739, 45
- Genzel, R., Tacconi, L. J., Gracia-Carpio, J., et al. 2010, MNRAS, 407, 2091
- Genzel, R., Newman, S., Jones, T., et al. 2011, ApJ, 733, 101
- Hainline, K. N., Shapley, A. E., Greene, J. E., Steidel, C. C., Reddy, N. A., & Erb, D. K. 2012, ApJ, 760, 74
- Hopkins, A. M., & Beacom, J. F. 2006, ApJ, 651, 142
- Ilbert, O., McCracken, H. J., Le Fevre, O., et al. 2013, arXiv:1301.3157
- Jones, T. A., Swinbank, A. M., Ellis, R. S., Richard, J., & Stark, D. P. 2010, MNRAS, 404, 1247
- Kennicutt, Jr., R. C. 1998, ApJ, 498, 541
- Kewley, L. J., & Dopita, M. A. 2002, ApJS, 142, 35

- Kewley, L. J., & Ellison, S. L. 2008, *ApJ*, 681, 1183
- Lara-López, M. A., Cepa, J., Bongiovanni, A., et al. 2010, *A&A*, 521, L53
- Lehnert, M. D., Nesvadba, N. P. H., Le Tiran, L., et al. 2009, *ApJ*, 699, 1660
- Lehnert, M. D., Le Tiran, L., Nesvadba, N. P. H., et al. 2013, *A&A*, 555, A72
- Le Tiran, L., Lehnert, M. D., van Driel, W., Nesvadba, N. P. H., & Di Matteo, P. 2011, *A & A*, 534, L4
- Liu, X., Shapley, A. E., Coil, A. L., Brinchmann, J., & Ma, C.-P. 2008, *ApJ*, 678, 758
- Maiolino, R., Nagao, T., Grazian, A., et al. 2008, *A&A*, 488, 463
- Mannucci, F., Cresci, G., Maiolino, R., Marconi, A., & Gnerucci, A. 2010, *MNRAS*, 408, 2115
- Mannucci, F., Cresci, G., Maiolino, R., et al. 2009, *MNRAS*, 398, 1915
- Muzzin, A., Marchesini, D., Stefanon, M., et al. 2013, *arXiv:1303.4409*
- Newman, S. F., Shapiro Griffin, K., Genzel, R., et al. 2012, *ApJ*, 752, 111
- Newman, S. F., Buschkamp, P., Genzel, R., et al. 2013, *arXiv:1306.6676*
- Noeske, K. G., Weiner, B. J., Faber, S. M., et al. 2007, *ApJ*, 660, L43
- Oey, M. S., & Clarke, C. J. 1997, *MNRAS*, 289, 570
- Penston, M. V., Robinson, A., Alloin, D., et al. 1990, *A&A*, 236, 53
- Richard, J., Jones, T., Ellis, R., et al. 2011, *MNRAS*, 413, 643
- Rigby, J. R., Wuyts, E., Gladders, M. D., Sharon, K., & Becker, G. D. 2011, *ApJ*, 732, 59
- Shirazi, M., & Brinchmann, J. 2012, *MNRAS*, 421, 1043
- Shirazi, M., Vegetti, S., Nesvadba, N., et al. 2013, submitted to *MNRAS*, *arXiv:1306.6282*
- Swinbank, A. M., Webb, T. M., Richard, J., et al. 2009, *MNRAS*, 400, 1121
- Tacconi, L. J., Genzel, R., Neri, R., et al. 2010, *Nature*, 463, 781
- Tacconi, L. J., Neri, R., Genzel, R., et al. 2013, *ApJ*, 768, 74
- Tremonti, C. A., Heckman, T. M., Kauffmann, G., et al. 2004, *ApJ*, 613, 898
- Verdolini, S. and Yeh, S. C. C. and Krumholz, M. R. and Matzner, C. D. and Tielens, A. G. G. M., 2013, *ApJ*, 769, 12

- Wisnioski, E., Glazebrook, K., Blake, C., et al. 2012, MNRAS, 422, 3339
- Wuyts, E., Rigby, J. R., Sharon, K., & Gladders, M. D. 2012, APJ, 755, 73
- Yeh, S. C. C., & Matzner, C. D. 2012, ApJ, 757, 108
- York, D. G., Adelman, J., Anderson, Jr., J. E., et al. 2000, AJ, 120, 1579

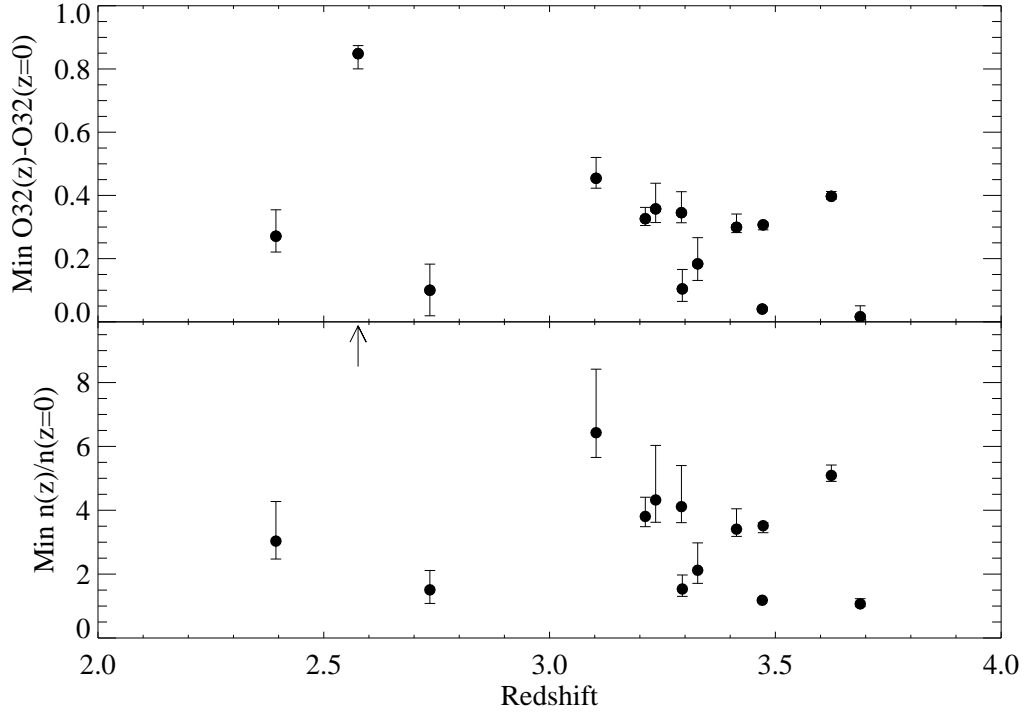


Fig. 4.— Top panel: The minimum difference in O32 between the high- and low- z samples when corrected for metallicity as described in the text. Bottom panel: The resulting minimum density difference between the high- and low- z samples when corrected for metallicity.